Chapter III

Effect of Gamma rays and 90 MeV Carbon Ion Beam Irradiation on Optical, Luminescence, and Electrical Properties of Polystyrene/Al_2O_3 Polymer Nanocomposites

This chapter gives an account of the study of optical, luminescence, electrical, thermal properties, and surface morphology of Al_2O_3/Polystyrene polymer nanocomposites at a different level of nanoparticles. The various properties of polymer nanocomposites have been studied before and after gamma rays and carbon ion beam irradiations.

3.1 Introduction

The polymer has recently become an attractive host material because of its usefulness in applications in integrated optical devices, electrical shielding for computer, light reflectors in cars, packaging, on-chip inter-connectors, etc. and its advantages in terms of low cost, non-corrosiveness, dielectric tenability, flexibility and mechanical strength [1–4]. They are useful not only to stabilize nanoparticles but also to change nanoparticles' surface nature [5]. Among all, polystyrene is one of the most commercially available polymers. It has low density, high thermal resistance, excellent mechanical durability, and ease of moulding and processing [6]. Polymer with metal oxide nanoparticles as fillers has especially gained more attention in many industrial applications due to their controllable chemical and physical properties. The polymer's physical and chemical properties such as mechanical, optical, thermal, luminescence, electrical properties, etc., could also be improved by including metal oxide nanoparticles. The modifications of the polymer's physical and chemical properties strongly depend on the interfacial interaction between a nanofiller and the polymer [7]. In particular, Al_2O_3 is widely used in the microelectronics industry owing to its excellent mechanical, thermal, and electrical properties. Additionally, it has high wear resistance, high adsorption capacity, thermal stability, and abrasiveness [8]. It is widely used to improve the thermo-physical and ionic conductivity of solid polymer electrolytes. But few reports are available for Al_2O_3 nanoparticles doped polymer nanocomposites [8]. Thus, Al_2O_3 has been used as a nanofiller in the present investigation.

There are several well-known processes for altering the properties of polymer nanocomposites. Among all the methods, the irradiation technique is widely employed because of its advantages over other processes. Irreversible changes in the macroscopic properties of the polymer can be detected by exposure to radiation. During ion beam irradiation, some significant events do take place, such as chain scission and cross-linking, mass losses, electronic excitation, and ionization [9]. The interaction of swift heavy ions with target atoms is affected through the collision processes that lead to excitation of target electrons and ionization of target atoms. The projectile range of swift heavy ions is a few hundred micrometres, and the fluence required for a polymer to undergo structural changes in the range of 10^{11} to 10^{13} ions/cm^2. An additional characteristic of swift

heavy ions is that the deposition of energy is not uniform. This means high doses imparted in the vicinity of ion trajectory and low doses in the rest of the area [10]. In comparison, gamma irradiation has been found to have the capability to span over the entire area of the sample and is often expected to induce homogeneous changes [11]. These polymeric films were prepared with varying concentrations, namely, 1 to 4 wt% of Al_2O_3 nanoparticles using the solution casting method. The prepared films of 1, 2, 3, and 4 wt% Al_2O_3 doped PS were denoted here as PA1, PA2, PA3, and PA4, respectively. These samples were irradiated with gamma rays and also with 90 MeV C-ions at Inter-University Accelerator Centre, New Delhi. These pristine and irradiated samples were characterized using different techniques, as discussed in Chapter 2.

The variation of electrical, luminescence and optical properties of PS/Al_2O_3 nanocomposites has been discussed as a function of filler level and dose of gamma rays and SHI irradiations [12-14].

3.2 Results and Discussion

3.2.1 XRD Analysis

Figure 3.1 shows XRD patterns of pure PS and its composites. The diffraction patterns of PS/Al_2O_3 nanocomposites show a broad peak at 2Θ=19.76°, suggesting that the polymeric film is partially crystalline with a leading amorphous phase [11].

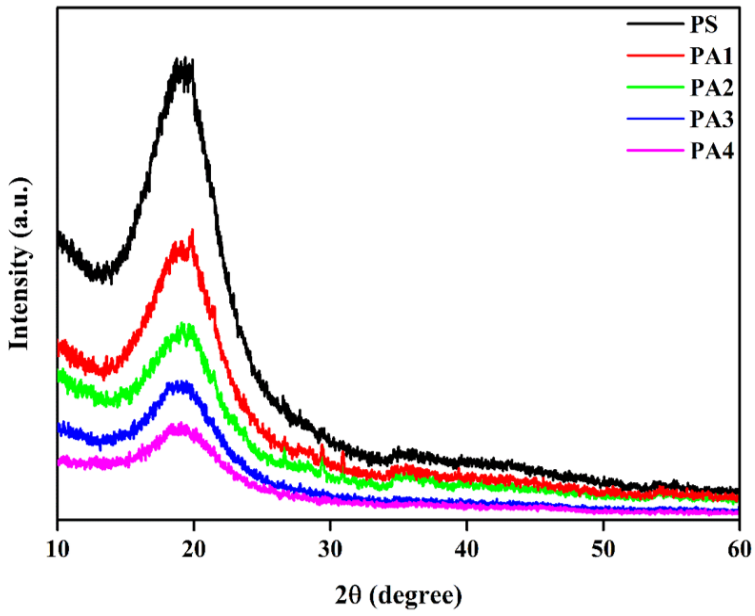

Figure 3.1 XRD patterns of PS/ Al_2O_3 films.

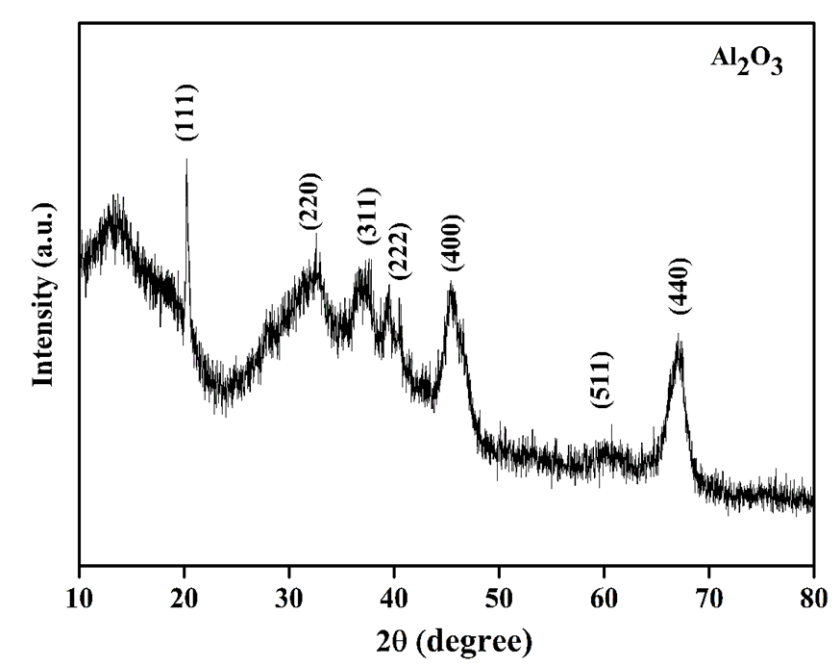

Figure 3.2 XRD patterns of Al_2O_3 nanoparticles.

The XRD pattern of Al_2O_3 shows the peaks around 2Θ=20°, 32°, 37°, 40°, 45.7°, 60.3° and 66.9°, as shown in figure 3.2. These peaks correspond to the cubic structure and are identified with (111), (220), (311), (222), (400), (511), and (440) reflections, respectively (JCPDS 29-0063). The inclusion of Al_2O_3 nanoparticles does not alter the XRD pattern of PS. Also, no other peaks are found in the XRD pattern of PS. Such a result has also been reported for PEO-Al_2O_3 composites by Jeewan et al. [8].

3.2.2 Energy Dispersive X-ray Analysis

Energy Dispersive X-ray analysis is employed to determine the elemental composition of polymer nanocomposites. The EDAX patterns of PS/Al_2O_3 polymer nanocomposites (figures 3.3 & 3.4) indicate the weight percentages of C, O, and Al, as listed in Table 3.1.

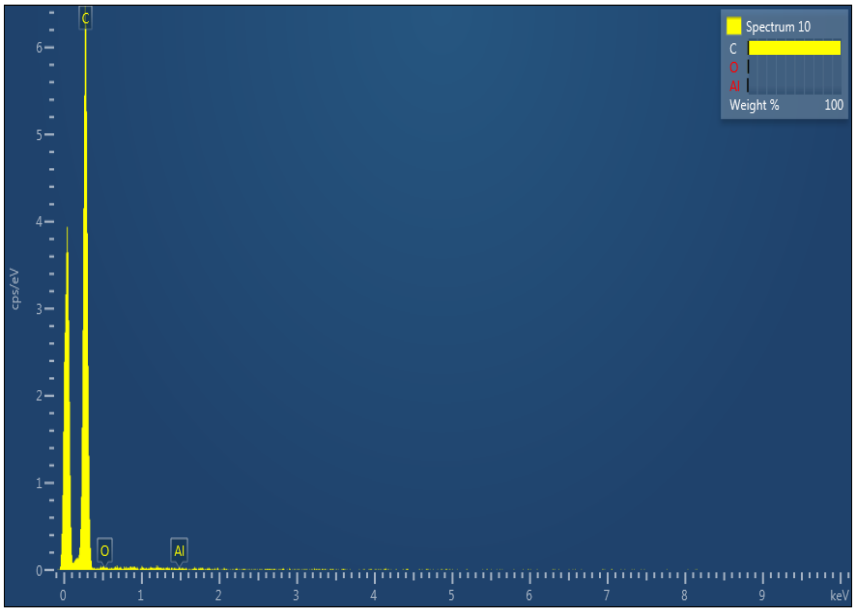

Figure 3.3 EDAX spectrum of PA2.

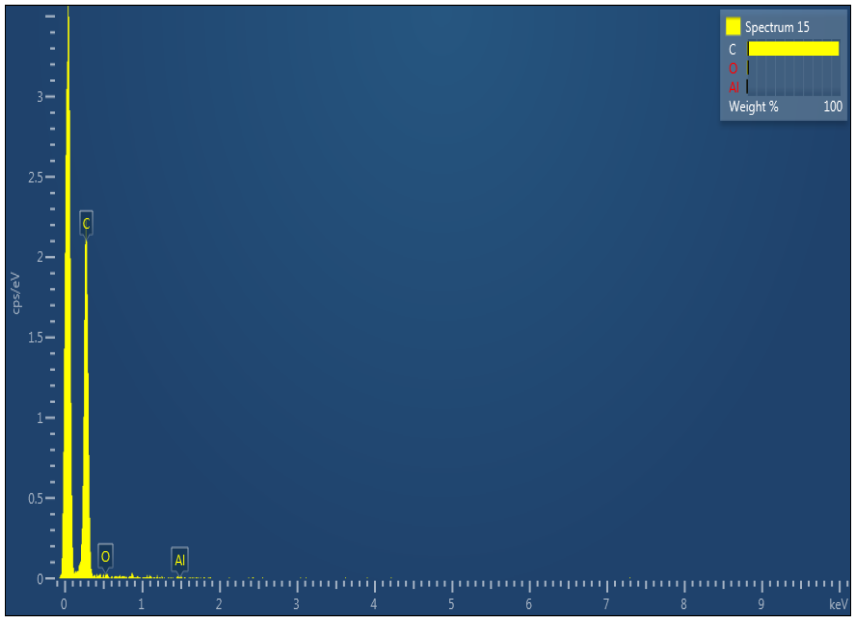

Figure 3.4 EDAX spectrum of PA4.

Element	wt% for PA2	wt% for PA4
C	98.99	98.23
O	0.86	1.38
Al	0.15	0.39
Total	100	100

Table 3.1 EDAX analysis of PA2 and PA4 films.

3.2.3 Fourier Transform Infrared Spectroscopy

Figures 3.5, 3.6 & 3.7 represent FTIR spectra of pristine and irradiated PS/Al_2O_3 polymer nanocomposites. For pure polystyrene, the presence of two bands at 906 and 979 cm^{-1} are assigned to the C–H rocking mode and C–C stretching mode, respectively. The vibrational bands at 1451 and 1496 cm^{-1} are related to the C-C stretching mode. The appearance of two bands in the range of 3000–2800 cm^{-1} corresponds to C-H bond stretching of saturated alkane. The bands at 757 and 1583 cm^{-1} are related to the out-of-plane C–H bending in the benzene ring and –CH_2 wagging mode, respectively.

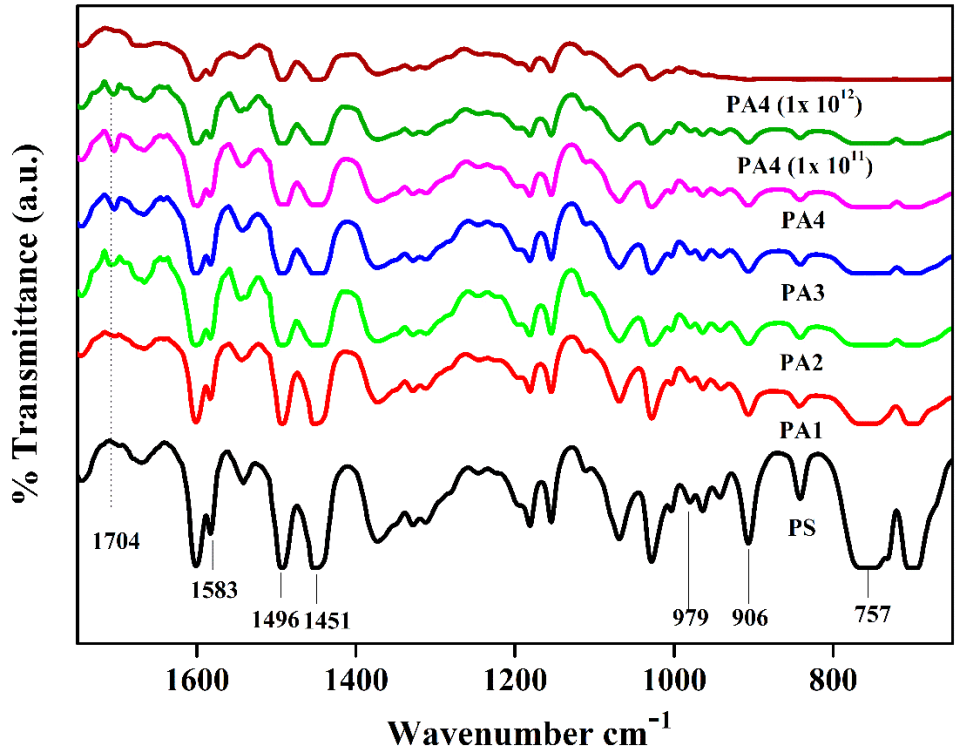

Figure 3.5 The FTIR spectra of pristine and irradiated polymeric films in the range of 700-1750 cm^{-1}.

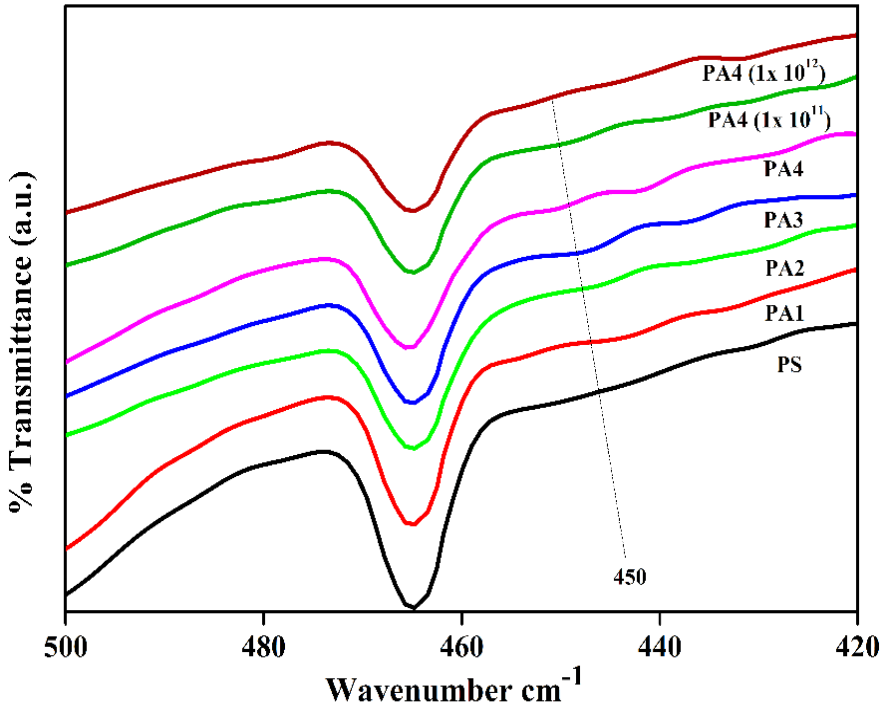

Figure 3.6 The FTIR spectra of pristine and irradiated nanocomposites in the range of 420-500 cm^{-1}.

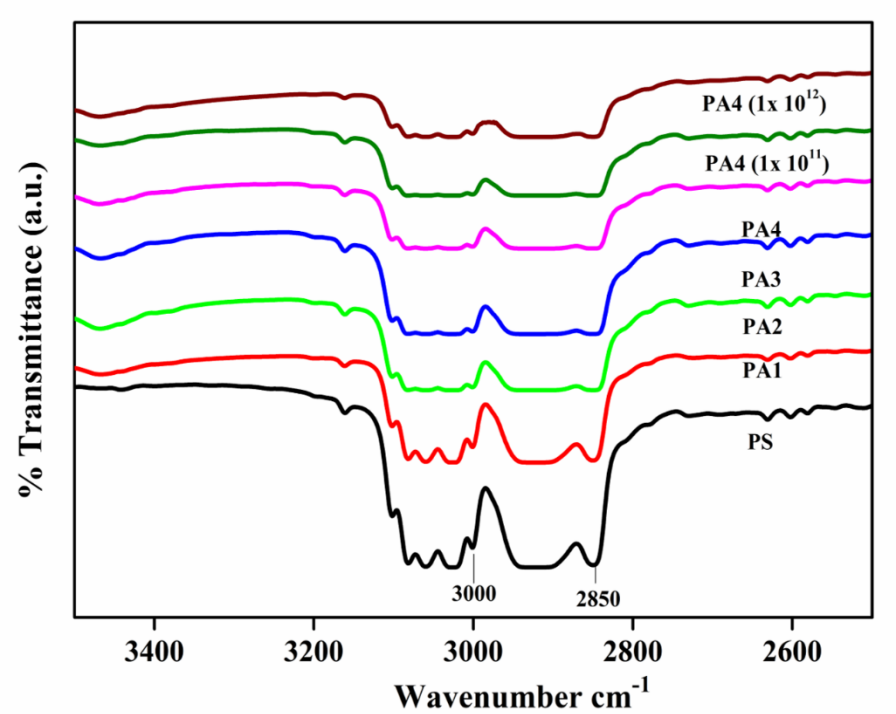

Figure 3.7 FTIR spectra of pristine and irradiated polymeric films in the range of 2500-3500 cm^{-1}.

The inclusion of nanoparticles reduces the intensity of all the peaks (as shown in figures 3.5, 3.6 & 3.7), indicating polymer-nanoparticles interaction.

The two new bands at 450 and 1704 cm^{-1} appeared in the FTIR spectra of PS/Al_2O_3 polymer nanocomposite films are assigned to stretching vibration of Al-O bond and C=O group, respectively [15]. It is observed that the intensity of all vibrational bands is reduced due to SHI irradiation. However, no significant change is observed after gamma irradiation. This is due to the benzene ring in polystyrene, which is not destroyed at the highest dose of gamma irradiation. Also, the presence of benzene rings in the polymer indicates radiation stability [16]. Upon SHI irradiation, a decrease in peaks' intensity can be explained as a change in the bond structure. This change in bond structure is caused by the extraction of hydrogen connected to the side and main chains of the polymer. These results imply degradation and randomization of the polymer chain.

3.2.4 UV-Visible Analysis

The optical absorption spectra of pristine and irradiated polymer nanocomposites were recorded in absorbance mode and are depicted in figure 3.8. The absorption in polystyrene may be related to the π- π* transition. The absorption edge of PS shows a significant shift towards the lower energy side as the filler level increases. This shifting of absorption edge can be attributed to chemical interaction between nanoparticles and polystyrene. Furthermore, after irradiation, red-shift observed in the absorption edge (ABE) of polymer nanocomposites is explained as forming new systems of extended conjugate bonds by breaking and forming new bonds. Post irradiation, the polymer films' colour changes from transparent to yellowish, indicating an increased density of the polymer chain [17–19].

Determination of Optical Bandgap:

The modification in the direct optical bandgap is determined by Tauc's formula [20].

$$\alpha h\nu = B\left(h\nu - E_g\right)^n$$

The direct bandgap (E_g) can be found by taking the intercept on the X-axis (the energy axis) of the plot $(\alpha h\nu)^2$ versus $h\nu$ and is given in Table 3.2. The bandgap of polystyrene is found to be 4.38 eV, which is observed to decrease with filler level and irradiation dose (Table 3.2).

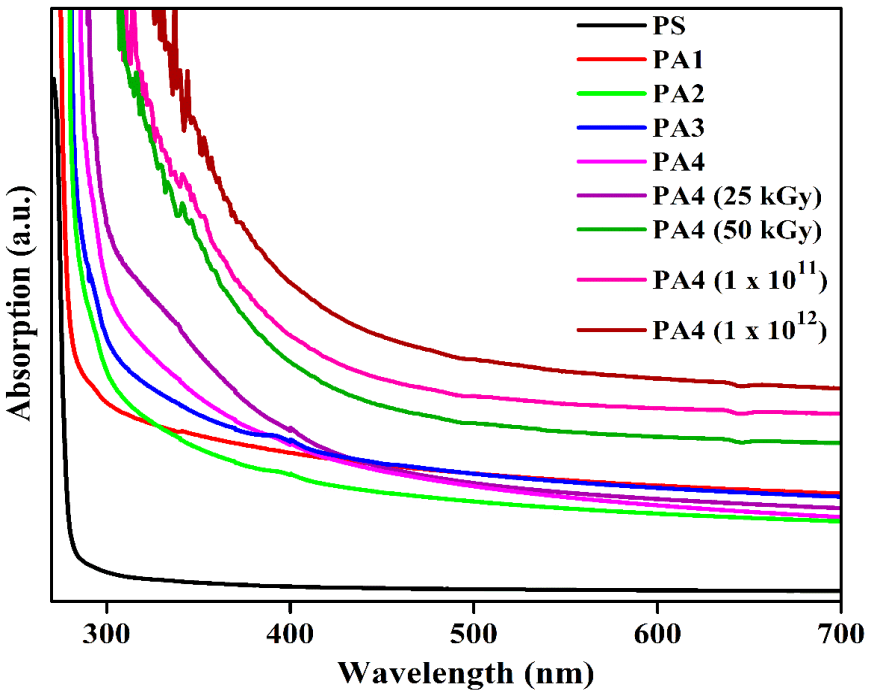

Figure 3.8 The absorption spectra of pure and doped PS and irradiated PA4.

A decrease in optical bandgap presumes due to the localized states' generation. The localized states' formation within the forbidden gap reduces the amount of energy for HOMO to LUMO transition [21–23]. The LET value of SHI irradiation is higher than that of gamma irradiation [24]. Hence, after SHI irradiation, the change in bandgap is more significant than that caused by gamma irradiation due to extremely high energy deposition in the case of SHI irradiation, the phenomenon is characterized by the density of state model in noncrystalline material as proposed by Mott and Davis [25]. According to this model, the host matrix disorder is accounted for a decrease in the bandgap, indicating increased conductivity. The number of C_6 rings in the cluster (M) was determined using the following equation [26].

$$E_g = 2\,|\beta|\,M^{-0.5}$$

$|\beta|$: Bond integral

The calculated value of M is reported in Table 3.2. From Table 3.2, it is seen that the value of M remains the same at low doses. At high fluence (1 x 10^{12} ions/cm^2) of SHI irradiation, M's value is 2, which is explained based on an increasing rate of dehydrogenation process [11].

Sample	Bandgap (eV)	Number of carbon hexagon rings
PS	4.38	~1
PA1	4.33	~1
PA2	4.28	~1
PA3	4.20	~1
PA4	4.09	~1
PA4 (25 kGy)	4.00	~1
PA4 (50 kGy)	3.45	~1
PA4 (1 x 10^{11})	3.77	~1
PA4 (1 x 10^{12})	3.19	~2

Table 3.2 Optical bandgap and number of C_6 ring in the cluster of pristine and irradiated polymeric films.

3.2.5 Photoluminescence

The photoluminescence property of PS/Al_2O_3 polymer nanocomposites was investigated for different concentrations of Al_2O_3 nanoparticles. Figure 3.9 depicts the excitation spectrum of polymeric films, observed at an emission wavelength of 435 nm. It shows a broad excitation band centred around 380 nm. The photoluminescence emission spectra of PS/Al_2O_3 polymer films were therefore recorded at an excitation wavelength of 380 nm, as shown in figure 3.10.

Figure 3.11 shows the Gaussian curve fitting of PL emission spectra of pure PS. It comprises three peaks centred at 411 nm, 435 nm, and 462 nm in the violet-blue region. It has been reported that the PL emission spectrum of polystyrene is due to the development of benzoic acid, styrene, methyl benzoate, stilbene-like luminescence substance upon absorption of 380 nm wavelength [27]. The intensity of the PL emission peaks has been observed to increase with the increase in filler levels. It is because of highly populated allowed electronic transition. This electronic transition enhances due to the filler level.

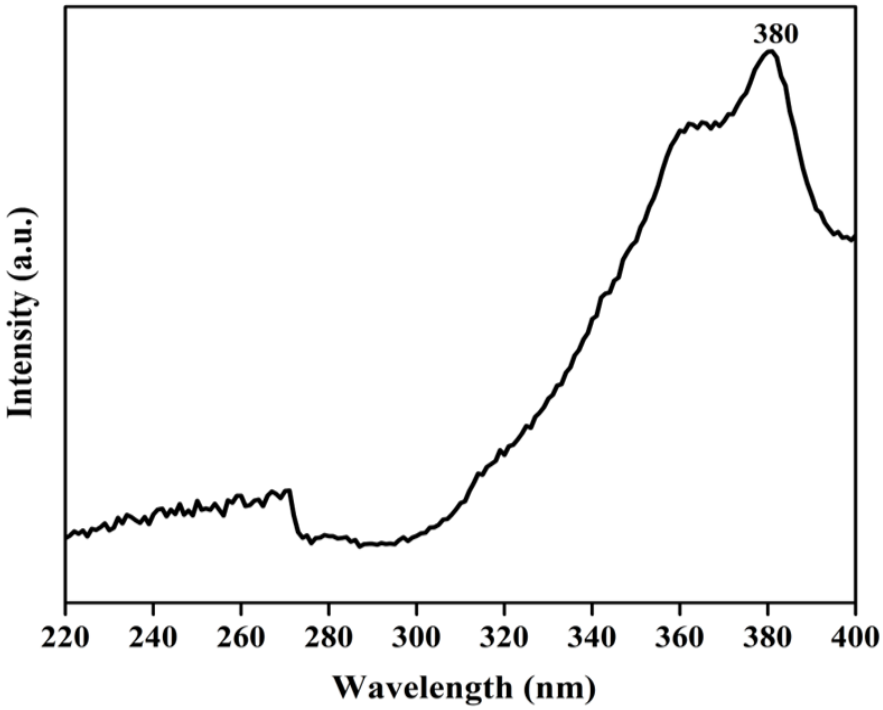

Figure 3.9 PL excitation spectra of PS at the emission wavelength of 435 nm.

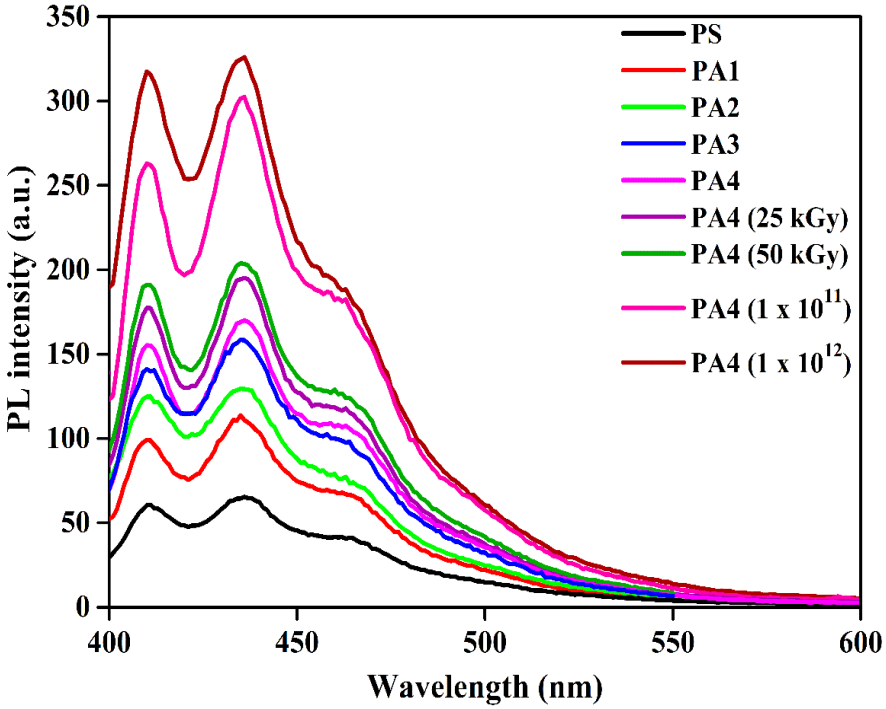

Figure 3.10 PL emission spectra of pristine and irradiated PS-based polymer nanocomposites at an excitation wavelength of 380 nm.

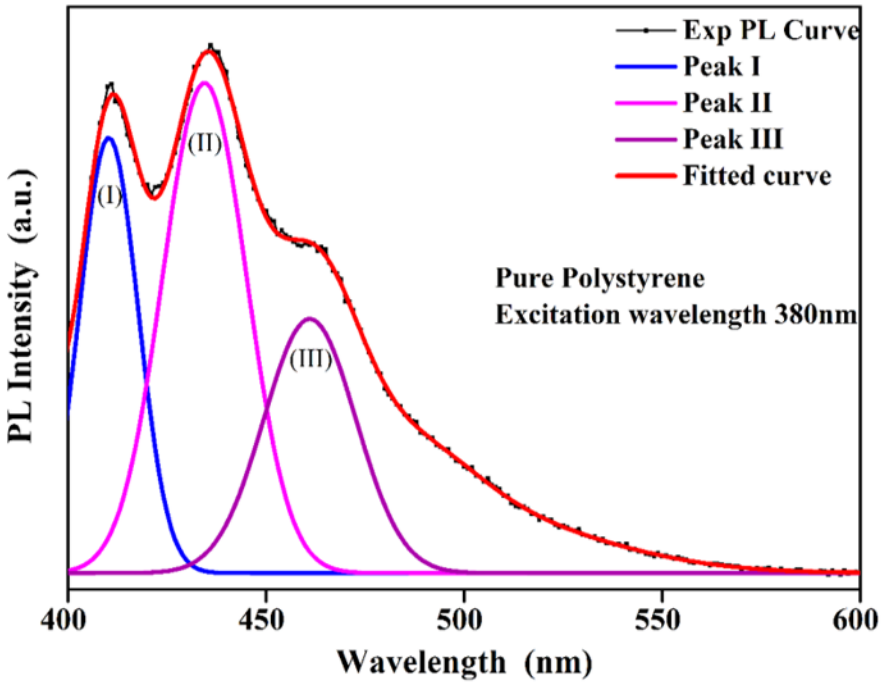

Figure 3.11 Gaussian fitting of the photoluminescence emission spectrum of pure polystyrene.

Further, the increase in the intensity of PL emission peaks is observed due to gamma and 90 MeV C^{6+} ion beam irradiations. It indicates that new radiative recombination occurs as a result of irradiation. This new radiative recombination is associated with dose, resulting in a change in the facial layer's configuration. Hence, the rate of radiation transition escalates with dose [28,29]. Also, irradiations produce a carbon cluster and reduce hydrogen concentration from the main and side groups of polymer matrices. This reduction in hydrogen concentration may be the result of the bonds' scission and is one of the reasons for the increase in PL emission intensity [30]. From figure 3.10, it is clear that the effect of SHI irradiation on PL emission intensity of polymer is higher than that of gamma irradiation. This means that SHI irradiation produces more defects than gamma irradiation does. These defects act as radiative centers, implying increasing PL emission intensity.

3.2.6 Thermoluminescence

Thermoluminescence glow curves of gamma and 90 MeV C^{6+} ions irradiated PS/Al_2O_3 polymer nanocomposites are illustrated in figures 3.12 & 3.13, respectively. Thermoluminescence is employed to investigate the dosimetry properties of ionizing radiation. Irradiation is a technique to produce charge

carriers; most of these charge carriers recombine and produce luminescence that can be noticed directly after irradiation. But some of these charge carriers get sufficient energy to divert from recombination. Successive trapping of these charge carriers can occur at trapping sites, which are released by subsequent heating. They recombine radiatively and dissipate their energy in the form of light, which results in TL maxima. TL glow curves of polymer composites comprise several TL maxima associated with different molecular relaxations, namely δ-,γ- and β - relaxations. Two T_ms were observed.

According to maximum temperatures at maximum intensity criterion, the detrapping of charge carriers occurs through γ -relaxation, which is correlated to the methylene group's torsion motion, created in the backbone of polystyrene by head to head and tail to tail pairing [31].

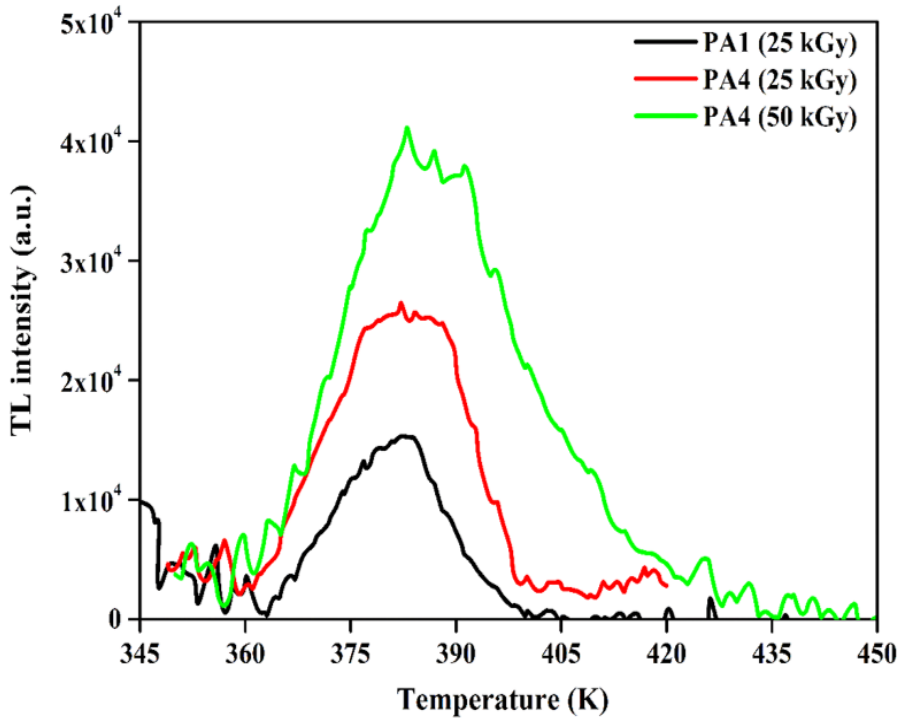

Figure 3.12 TL glow curves of gamma-irradiated polymer composites.

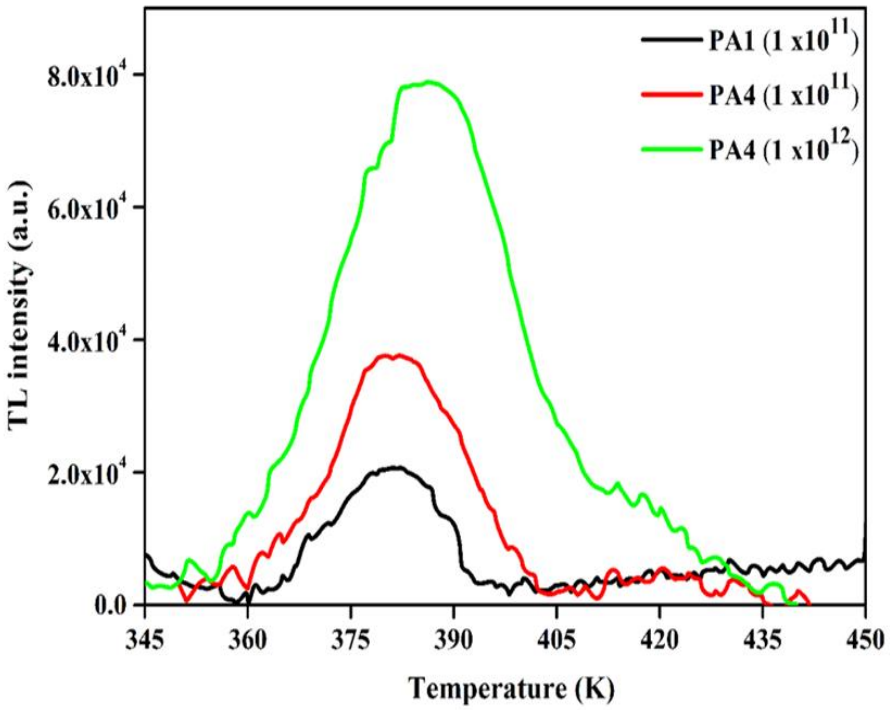

Figure 3.13 TL glow curves of 90 MeV Carbon ions irradiated polymer composites.

Various methods are known for studying the yield of TL glow curves. GCD fitting method is the most used for the analysis of complex glow curves among all methods. Figure 3.14 shows GCD fitting of TL glow curves of PA4 polymeric film. This fitting was carried out using the equation of general order kinetics, given by Kitis et al. [32]. Kitis et al. equation for general order kinetics are as follows:

$$I(T) = I\,m\,b^{b-1}\,exp\left(\frac{E}{kT}\times\frac{T-Tm}{Tm}\right)\times\left((b-1)\frac{T^2}{Tm^2}\left(1-\frac{2kT}{E}\right)exp\left(\frac{E}{kT}\times\frac{T-Tm}{Tm}\right)+1+(b-1)\frac{2kTm}{E}\right)^{-\frac{b}{b-1}}$$

$$s = \frac{\beta E_a}{k_B T_m^2\left[1+\frac{2k_B T_m(b-1)}{E_a}\right]}\exp\left(\frac{E_a}{k_B T_m}\right)$$

where, b = kinetic parameter, s = frequency factor, E = activation energy k = Boltzmann's constant, T_m = temperature at maximum intensity I_m.

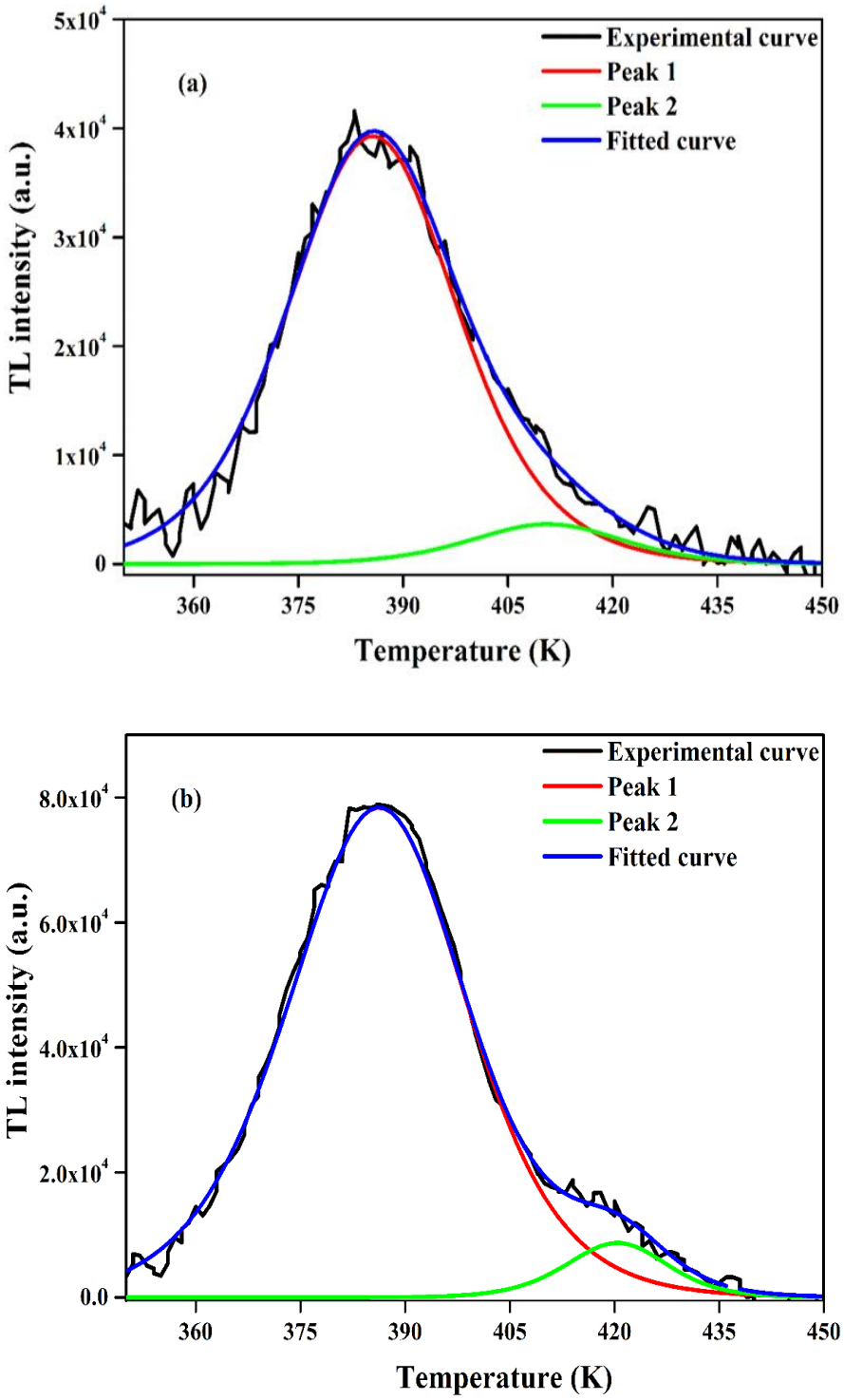

Figure 3.14 GCD fitting of TL glow curves of (a) Gamma irradiated PA4(50 kGy) (b) SHI irradiated PA4($1x10^{12}$).

Samples	Fluence	Peak	T_m (K)	E (eV)	B	s (s^{-1})
PA4 (gamma irradiated)	50 kGy	1	385.6	1.425	1.796	2.69 x 10^{17}
		2	410.6	1.776	1.744	4.30 x10^{20}
PA4 (SHI beam irradiated)	1×10^{12} ions/cm^2	1	380.2	1.32	1.712	3.66x 10^{15}
		2	420.4	2.9	1.79	7.06 x 10^{32}

Table 3.3 Kinetic parameter and activation energy for glow, as calculated from GCD for irradiated PA4 films.

Values of all parameters of the fitted curve are given in Table 3.3. The value of activation energy is observed to vary from 1.32 eV to 1.776 eV, whereas the value of b corresponds to the general order kinetics. TL glow curve intensity shows an increase with irradiation dose, which may indicate an increase in the number of trapping centers upon irradiation. Moreover, the change in the intensity of the TL glow curve for SHI irradiated samples is more pervasive than for gamma-irradiated ones. It could be concluded that the energy deposited by gamma rays and C^{6+} ions formed similar types of defects and trapping centers at various depths in polymer nanocomposites [33].

3.2.7 AC Electrical Properties

3.2.7.1 Dielectric Constant

The dielectric studies are used to understand molecular relaxation behaviour and conductivity mechanism of polymer nanocomposites. Figure 3.15 depicts the variation of the dielectric constant of pristine and irradiated polymer nanocomposites. The value of the dielectric constant is high at low frequencies and becomes constant at high frequencies. The result complies with the long-range orientation of free radicals and the expected response of existing dipoles in the presence of a slow varying electric field at lower frequencies [29,30,34]. At higher frequencies, the charge density tends to decrease at the interface due to the slower response of dipoles as well as the short drift of charge carriers with a rapidly varying electric field, resulting in the decrease of dielectric constant values [8,35].

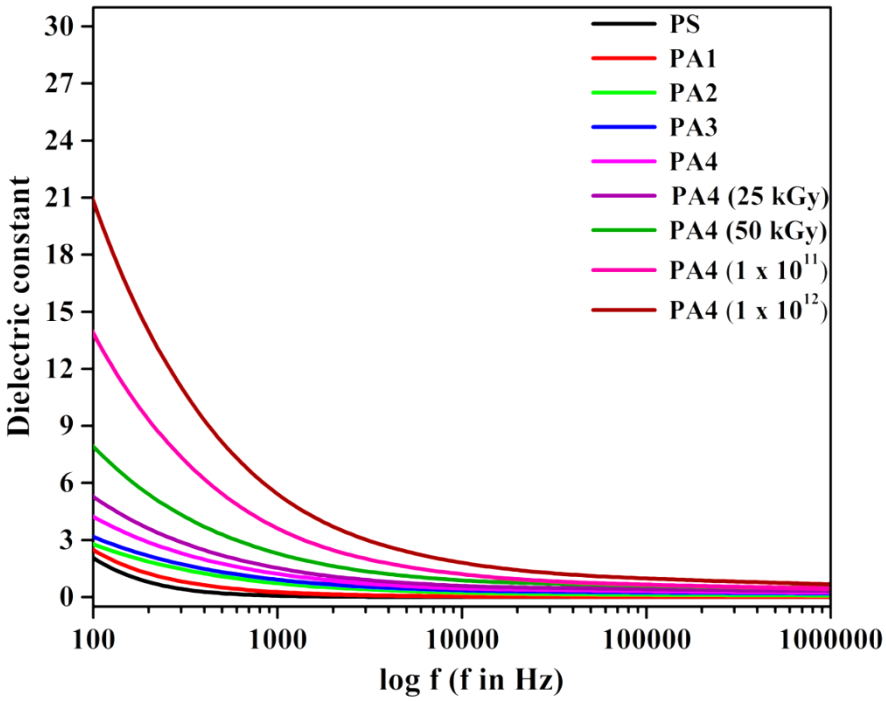

Figure 3.15 Dielectric constant vs frequency of polymer nanocomposites with the concentration of filler and the dose.

As the filler concentration increases, dielectric constants' overall response increases due to the interfacial polarization effect between filler and polymer matrices. Moreover, an increase in the dielectric constant with irradiation dose indicates the formation of low molecular polymeric macromolecules in the lower frequency region. The reason for the rise in dielectric constant is the formation of defects and an increase in charge density after both types of irradiations, as discussed in optical studies (section 3.2.4) [19]. This indicates that SHI irradiation stimulates significant degradation of polymer nanocomposites and, therefore, increases the dielectric constant value.

3.2.7.2 Dielectric Loss

The dielectric loss is the dissipation of power as heat when a dielectric material is placed in an electric field. Figure 3.16 presents the variation in dielectric loss of pre and post-irradiated PS/Al_2O_3 films with frequency. Figure 3.16 shows that the dielectric loss varies exponentially at lower frequencies; subsequently, with increasing frequency, it weakly depends on frequency. As frequency increases, the induced charges fail to follow the rapidly reversing field, implying a decrease in ionic oscillations [36].

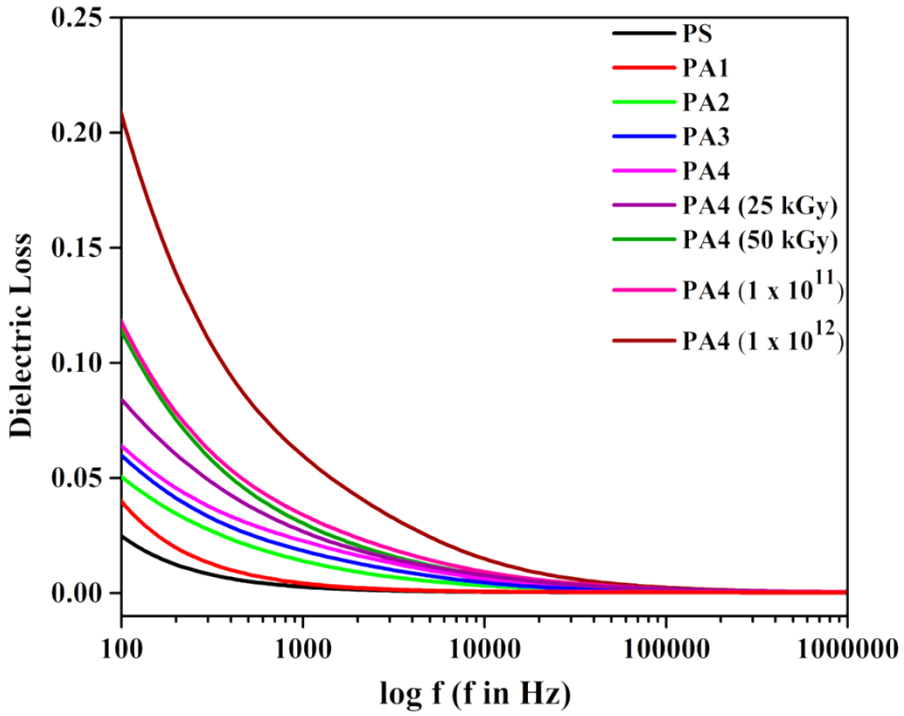

Figure 3.16 Variation in the dielectric loss versus frequency for polymer nanocomposites with the concentration of filler and dose.

Furthermore, the dielectric loss increases moderately with increasing filler level due to the interfacial polarization mechanism of PS/Al_2O_3 system. The overall values of dielectric loss are enhanced with gamma and SHI irradiations, attributable to the escalating number of charge carriers due to irradiation [37].

3.2.7.3 AC Electrical Conductivity

AC conductivity of PS/Al_2O_3 polymeric films was studied as a function of frequency, filler level, and irradiation dose. The results are shown in figure 3.17. The conductivity of polystyrene increases with increasing filler levels. This can be ascribed to the electronic interaction between nanofiller and polystyrene [38]. At low frequencies, the charge transport extends over a long distance, but at the same time, it is limited to isolated conducting regions. So overall conductivity is low. However, at high frequencies, the charge transport extends over a longer distance due to the applied electric field force. With increased frequency, the hopping mechanism becomes more effective, resulting in increased conductivity [39]. After irradiation, the increase in the conductivity is observed due to the promotion of bonding of nanofiller to polymer and alteration of polymeric structure to carbon enrich the network. This carbon enrich network is formed due to the emission of hydrogen and volatile gases during irradiation [40–42].

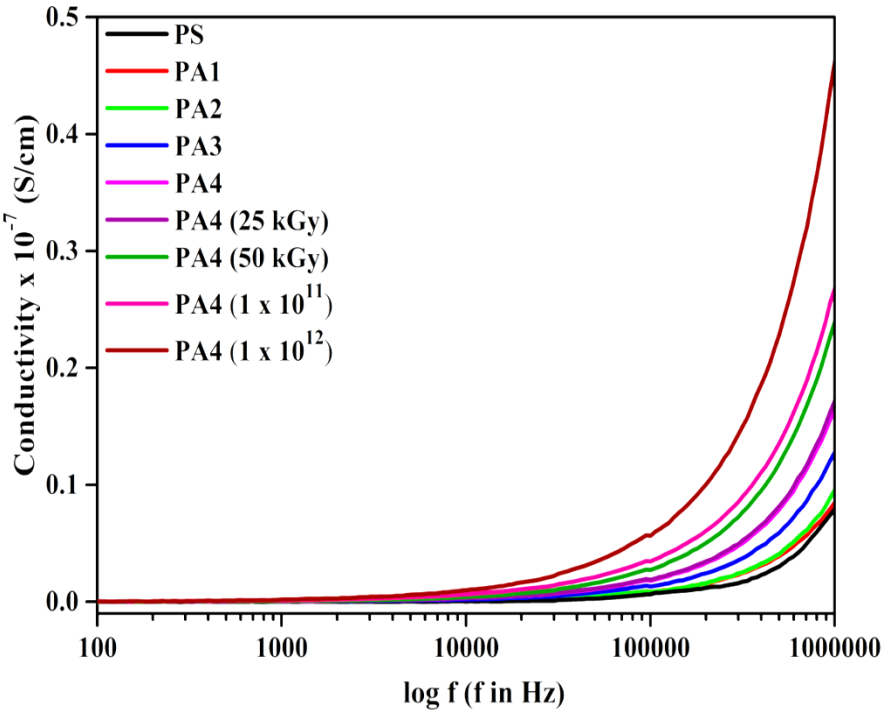

Figure 3.17 Variation in AC conductivity with frequency for polymer nanocomposites at various filler concentrations and doses

An increase in the amount of local energy deposition with gamma irradiation dose and ion fluence indicates an increase in free electrons and impurities. Therefore, due to the lower value of linear energy transfer of gamma radiation than SHI irradiation, there is a minimal change in the value of conductivity of gamma-irradiated samples [11].

3.2.8 Differential Scanning Calorimetry Analysis

The polymer's glass transition temperature is an important property that is defined as the temperature at which the polymer converts into a fragile state when it cools after heating. The polymer chains are interconnected through weak secondary bonds. At glass transition temperature, these bonds break down, and the motion of macromolecules sets in. The filler and irradiation effect on the glass transition temperature of polystyrene was studied using differential scanning calorimetry technique (DSC), as shown in figure 3.18. The glass transition temperature of pure polystyrene is observed to be ~335.4 K. It migrates to a higher temperature as nanofillers' concentration increases. This suggests the strong interaction of polystyrene with nanoparticles and explains the constraint on the macromolecular motion [43].

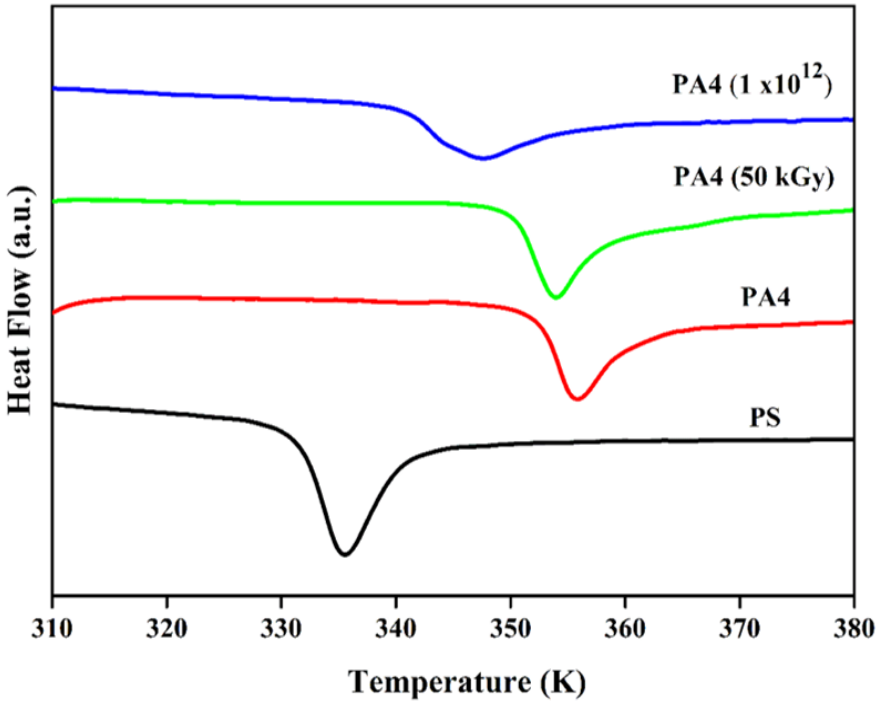

Figure 3.18 DSC thermograms of PS, pristine and irradiated PA4.

After irradiation, the glass transition temperature of PA4 is observed to shift to a lower value, which may be due to the increased polymeric chain's mobility and, therefore, free volume. The formation of extra free volume promotes the large-scale segmental motion of polymeric material [39]. Thus, it could be imperative to conclude that the macromolecular motion increases with the irradiation dose, and it is an effect of chain scission of the polymer matrix. Moreover, polymer nanocomposites become more disordered due to irradiation. These results relate to results obtained from FTIR and UV-visible analysis.

3.2.9 Surface Morphology

AFM images of pristine PS and PA4 and also irradiated PA4, of areas ~ 5 x 5 μm^2 are shown in figure 3.19. They have been analyzed in terms of average surface roughness (R_a). The average surface roughness of pristine PS and PA4 is observed to be 9 nm and 34 nm, respectively. The average surface roughness of PA4 irradiated with SHI at the fluence of 1 x 10^{12} ions per cm^2 is 6 nm, whereas that of the sample irradiated with 50 kGy gamma rays is ~31 nm. The incorporation of nanoparticles into polystyrene increases average surface roughness due to the increased density and size of nanoparticles on the surface of the film.

In contrast, the average surface roughness of PA4 decreases due to both the gamma rays and SHI irradiations. This could be due to the defect enhanced surface diffusion. Upon SHI irradiation, polymer nanocomposites become smoother than the gamma-irradiated samples. This is due to the energy deposition by SHI irradiation higher than by gamma irradiation.

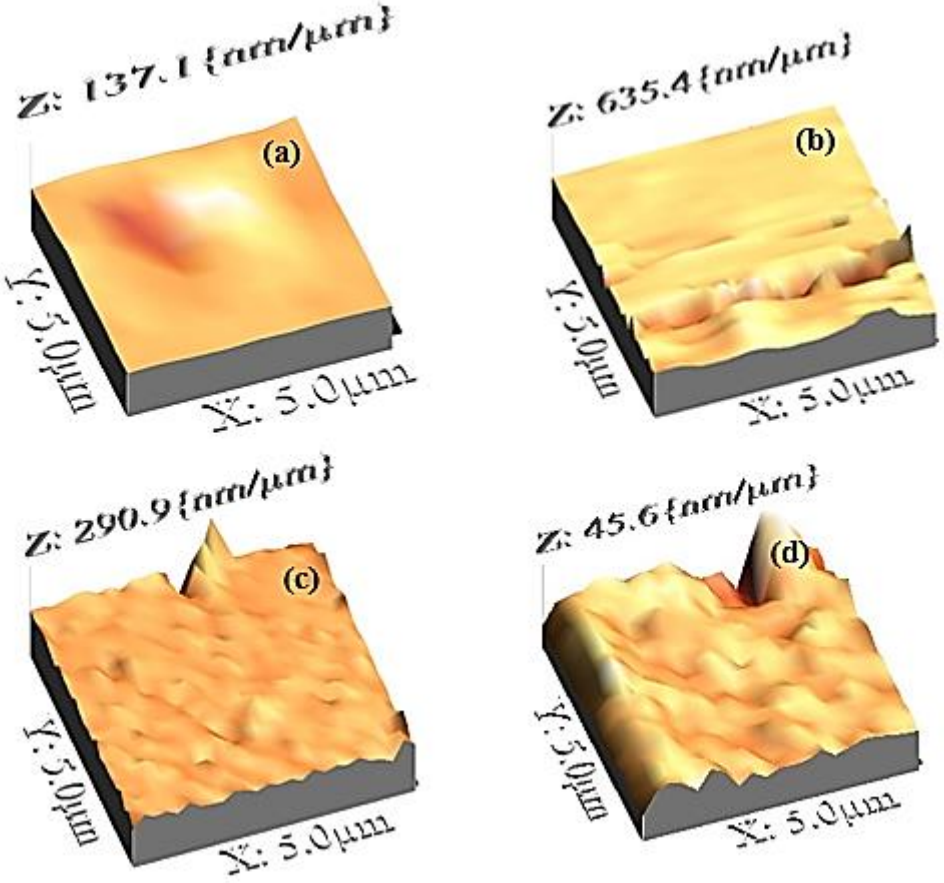

Figure 3.19 AFM images of (a) PS (b) PA4 (c) Gamma irradiated PA4 (50 kGy) and (d) SHI irradiated PA4 (1x 10^{12}).

3.3 Conclusion

No significant peak of Al_2O_3 is observed in XRD patterns of polymer nanocomposites. The EDAX spectra of polymer nanocomposites show the presence of nanoparticles in the polymer matrix. The optical bandgap of PS is observed to be 4.38 eV, which decreases with filler level and irradiation dose. The intensity of PL emission spectra increases with increasing filler concentration and irradiation dose due to the increase in the defect concentration. The overall response of dielectric constant and dielectric loss of pristine and irradiated polymer nanocomposites has been observed high compared to that of the pure PS due to the transformation of polystyrene structure into an enriched carbon

network. The glass transition temperature rises due to the inclusion of filler, whereas it decreases due to irradiation. Moreover, polymer's roughness is noticed to be high after incorporating nanoparticles and low after irradiation. Overall, it has been noticed that the effect of SHI irradiation on the physical-chemical properties of polymer nanocomposite is more significant than that of gamma irradiation. These results confirm that such high-energy radiation may be an effective and reliable method for improving the properties of polymer nanocomposites for luminescence application.

References:

[1] M. R. Becker, V. Stefani, R. R. B. Correia, C. Bubeck, M. Jahja, M. M. C. Forte, Waveguide optical properties of polystyrene doped with p - nitroaniline derivatives, Opt. Mat. 32 (2010) 1526–1531. https://doi.org/10.1016/j.optmat.2010.06.015.

[2] J. Deris, S. Hajati, Reflection electron energy loss spectroscopy as efficient technique for the determination of optical properties of polystyrene intermixed with gold nanoparticles, Appl. Surf. Sci. 392 (2017) 697–700. https://doi.org/10.1016/j.apsusc.2016.09.021.

[3] S. Hajati, V. Zaporojtchenko, F. Faupel, S. Tougaard, Characterization of Au nano-cluster formation on and diffusion in polystyrene using XPS peak shape analysis, Surf. Sci. 601 (2007) 3261–3267. https://doi.org/10.1016/j.susc.2007.06.001.

[4] J. Deris, S. Hajati, S. Tougaard, V. Zaporojtchenko, Determination of electronic properties of nanostructures using reflection electron energy loss spectroscopy: Nano-metalized polymer as case study, Appl. Surf. Sci. 377 (2016) 44–47. https://doi.org/10.1016/j.apsusc.2016.03.092.

[5] S. K. Tripathi, R. Kaur, Jyoti, Investigation of non-linear optical properties of CdS/PS polymer nanocomposite synthesized by chemical route, Opt. Commun. 352 (2015) 55–62. https://doi.org/10.1016/j.optcom.2015.04.042.

[6] Q. Tai, Y. Kan, L. Chen, W. Xing, Y. Hu, L. Song, Morphologies and thermal properties of flame-retardant polystyrene / a -zirconium phosphate nanocomposites, React. Funct. Polym. 70 (2010) 340–345. https://doi.org/10.1016/j.reactfunctpolym.2010.02.008.

[7] M. R. Mehrnia, Y. M. Mojtahedi, M. Homayoonfal, What is the concentration threshold of nanoparticles within the membrane structure? A case study of Al_2O_3/PSf nanocomposite membrane, Desalination. 372 (2015) 75–88. https://doi.org/10.1016/j.desal.2015.06.022.

[8] R. J. Sengwa, S. Choudhary, Dielectric and electrical properties of PEO–Al_2O_3 nanocomposites, J. Alloys Compd. 701 (2017) 652–659. https://doi.org/10.1016/j.jallcom.2017.01.155.

[9] Z. Zhu, C. Liu, Y. Sun, J. Liu, Y. Tang, Y. Jin, J. Du, Modification of polyethylene terephthalate under high-energy heavy ion irradiation, Nucl.

Instruments Methods Phys. Res. Sect. B Beam Interact. with Mater. Atoms. 191 (2002) 723–727. https://doi.org/10.1016/S0168-583X(02)00641-9.

[10] M. Lagarde, A. De Paz, M. F. Del, D. Fasce, R. Dommarco, S. Laino, L. A. Fasce, On the comparison of changes induced in crystallinity and surface nanomechanical properties of ultra high molecular weight polyethylene by γ and swift heavy ion irradiations, Surf. Coat. Technol. 258 (2014) 293–299. https://doi.org/10.1016/j.surfcoat.2014.09.010.

[11] A. A. El-Saftawy, A. M. Abdel Reheem, S. A. Kandil, S. A. Abd El Aal, S. Salama, Comparative studies on PADC polymeric detector treated by gamma radiation and Ar ion beam, Appl. Surf. Sci. 371 (2016) 596–606. https://doi.org/10.1016/j.apsusc.2016.03.044.

[12] S. Bhavsar, G. B. Patel, N. L. Singh, Investigation of optical properties of aluminium oxide doped polystyrene polymer nanocomposite films, Phys. B Condens. Matter. 533 (2018) 12–16. https://doi.org/10.1016/j.physb.2017.12.055.

[13] S. Bhavsar, N. L. Singh, Influence of gamma radiation on optical properties of Al_2O_3 doped polystyrene polymer films, AIP Conference Proceedings (2020) 080056. https://doi.org/10.1063/5.0001829.

[14] S. Bhavsar, G. B. Patel, N. L. Singh, D. Singh, F. Singh, Effect of 90 MeV carbon ions on Optical, Luminescence and Electrical properties of PS/Al_2O_3 Polymer Nanocomposite, (To be communicate)

[15] E. M. Abdelrazek, Spectroscopic studies on the effect of doping with $CoBr_2$ and $MgCl_2$ on some physical properties of polyvinylalcohol films, Phys. B Condens. Matter. 403 (2008) 2137–2142. https://doi.org/10.1016/j.physb.2007.11.029.

[16] R. Mishra, S. P. Tripathy, D. Sinha, K. K. Dwivedi, S. Ghosh, D. T. Khathing, M. Müller, D. Fink, W. H. Chung, Optical and electrical properties of some electron and proton irradiated polymers, Nucl. Instruments Methods Phys. Res. Sect. B Beam Interact. with Mater. Atoms. 168 (2000) 59–64. https://doi.org/10.1016/S0168-583X(99)00829-0.

[17] G. B. Patel, N. L. Singh, F. Singh, Modification of chitosan-based biodegradable polymer by irradiation with MeV ions for electrolyte applications, Mater. Sci. Eng. B. 225 (2017) 150–159. https://doi.org/10.1016/j.mseb.2017.08.023.

[18] S. S. Gasaymeh, S. Radiman, L. Y. Heng, E. Saion, Gamma Irradiation Synthesis and Influence the Optical and Thermal Properties of Cadmium Sulfide (CdS)/ Poly (Vinyl Pyrolidone) Nanocomposites, Am. J. Appl. Sci. 7 (2010) 500–508.

[19] G. B. Patel, N. L. Singh, F. Singh, P. K. Kulriya, Effects of MeV ions on physicochemical and dielectric properties of chitosan / PEO polymeric blend, Nucl. Inst. Methods Phys. Res. B. 447 (2019) 68–78. https://doi.org/10.1016/j.nimb.2019.03.052.

[20] J. Tauc, R. Grigorovici, A. Vancu, Optical Properties and Electronic Structure of Amorphous Germanium, Phys. Status Solidi. 15 (1966) 627–637. https://doi.org/10.1002/pssb.19660150224.

[21] W. H. Eisa, Y. K. Abdel-Moneam, Y. Shaaban, A. A. Abdel-Fattah, A. M. Abou Zeid, Gamma-irradiation assisted seeded growth of Ag nanoparticles within PVA matrix, Mater. Chem. Phys. 128 (2011) 109–113. https://doi.org/10.1016/j.matchemphys.2011.02.076.

[22] N. V. Bhat, M. M. Nate, M. B. Kurup, V. A. Bambole, S. Sabharwal, Effect of γ-radiation on the structure and morphology of polyvinyl alcohol films, Nucl. Instruments Methods Phys. Res. Sect. B Beam Interact. with Mater. Atoms. 237 (2005) 585–592. https://doi.org/10.1016/j.nimb.2005.04.058.

[23] R. P. Chahal, S. Mahendia, A. K. Tomar, S. Kumar, γ-Irradiated PVA/Ag nanocomposite films: Materials for optical applications, J. Alloys Compd. 538 (2012) 212–219. https://doi.org/10.1016/j.jallcom.2012.05.085.

[24] E. Lee, G. Rao, L. Mansur, LET effect on cross-linking and scission mechanisms of PMMA during irradiation, Radiat. Phys. Chem. 55 (1999) 293–305. https://doi.org/10.1016/S0969-806X(99)00184-X.

[25] N. F. Mott, E. A. Davis, Electronic Processes in Non Crystalline Materials, Clarendon Press, Oxford, 1979.

[26] J. Robertson, E. P. O'Reilly, Electronic and atomic structure of amorphous carbon, Phys. Rev. B. 35 (1987) 2946–2957. https://doi.org/10.1103/PhysRevB.35.2946.

[27] T. Uchihara, M. Shiroma, K. Ishimine, Y. Tamaki, Photoluminescence developed from polystyrene and CdS/polystyrene nanocomposite films in picosecond time range by repetitional irradiation of excitation femtosecond pulses in PL up conversion measurements, J. Photochem. Photobiol. A

Chem. 213 (2010) 93–100. https://doi.org/10.1016/j.jphotochem.2010.05.006.

[28] S. Tóth, M. Füle, M. Veres, I. Pócsik, M. Koós, A. Tóth, T. Ujvári, I. Bertóti, Photoluminescence of ultra-high molecular weight polyethylene modified by fast atom bombardment, Thin Solid Films. 497 (2006) 279–283. https://doi.org/10.1016/j.tsf.2005.10.050.

[29] G. B. Hadjichristov, I. L. Stefanov, B. I. Florian, G. D. Blaskova, V. G. Ivanov, E. Faulques, Optical reflectivity study of silicon ion implanted poly (methyl methacrylate), Appl. Surf. Sci. 256 (2009) 779–786. https://doi.org/10.1016/j.apsusc.2009.08.059.

[30] S. B. Aziz, Z. H. Z. Abidin, Electrical Conduction Mechanism in Solid Polymer Electrolytes: New Concepts to Arrhenius Equation, J. Soft Matter. 2013 (2013) 1–8. https://doi.org/10.1155/2013/323868.

[31] E. Dobruchowska, L. Okrasa, I. Glowacki, J. Ulanski, G. Boiteux, The 'wet dog' effect in polymers as seen by thermoluminescence, Polym. 45 (2004) 6027–6035. https://doi.org/10.1016/j.polymer.2004.06.019.

[32] G. Kitis, J. M. Gomez-Ros, J. W. N. Tuyn, Thermoluminescence glow-curve deconvolution functions for first, second and general orders of kinetics, J. Phys. D. Appl. Phys. 31 (1998) 2636–2641. https://doi.org/10.1088/0022-3727/31/19/037.

[33] N. J. Shivaramu, B. N. Lakshminarasappa, F. Singh, E. Coetsee, H. C. Swart, Thermoluminescence response in ^{60}Co gamma rays, 100 MeV Si^{8+} and 150 MeV Au^{9+} irradiated Y_2O_3:Ho^{3+} nanophosphor, J. Alloys Compd. 778 (2019) 554–565. https://doi.org/10.1016/j.jallcom.2018.11.185.

[34] Y. N. Sudhakar, M. Selvakumar, D. K. Bhat, $LiClO_4$-doped plasticized chitosan and poly(ethylene glycol) blend as biodegradable polymer electrolyte for supercapacitors, Ionics 19 (2013) 277–285. https://doi.org/10.1007/s11581-012-0745-5.

[35] M. F. Shukur, R. Ithnin, H. A. Illias, M. F. Z. Kadir, Proton conducting polymer electrolyte based on plasticized chitosan – PEO blend and application in electrochemical devices, Opt. Mater. 35 (2013) 1834–1841. https://doi.org/10.1016/j.optmat.2013.03.004.

[36] N. L. Singh, S. Shah, A. Qureshi, K. P. Singh, V. Shrinet, P. K. Kulriya, A. Tripathi, Radiation-induced modification of organometallic compound

dispersed polymer composites, Radiat. Eff. Defects Solids. 163 (2008) 181–189. https://doi.org/10.1080/10420150701688537.

[37] T. Phukan, D. Kanjilal, T. D. Goswami, H. L. Das, Dielectric response of irradiated PADC polymer track detector, Nucl. Instruments Methods Phys. Res. Sect. B Beam Interact. with Mater. Atoms. 234 (2005) 520–524. https://doi.org/10.1016/j.nimb.2005.02.022.

[38] Z. M. Elimat, AC electrical conductivity of poly(methyl methacrylate)/carbon black composite, J. Phys. D. Appl. Phys. 39 (2006) 2824–2828. https://doi.org/10.1088/0022-3727/39/13/028.

[39] S. Ningaraju, A. P. Gnana Prakash, H. B. Ravikumar, Studies on free volume controlled electrical properties of PVA/NiO and PVA/TiO_2 polymer nanocomposites, Solid State Ionics. 320 (2018) 132–147. https://doi.org/10.1016/j.ssi.2018.03.006.

[40] A. Qureshi, D. Singh, N. L. Singh, S. Ataoglu, A. N. Gulluoglu, A. Tripathi, D. K. Avasthi, Effect of irradiation by 140 Mev Ag^{11+} ions on the optical and electrical properties of polypropylene/TiO_2 composite, Nucl. Instruments Methods Phys. Res. Sect. B Beam Interact. with Mater. Atoms. 267 (2009) 3456–3460. https://doi.org/10.1016/j.nimb.2009.07.016.

[41] N. L. Singh, A. Sharma, D. K. Avasthi, V. Shrinet, Temperature and frequency dependent electrical properties of 50 MeV Li^{3+} ion irradiated polymeric blends, Radiat. Eff. Defects Solids. 160 (2005) 99–107. https://doi.org/10.1080/10420150500116649.

[42] D. Fink, W. H. Chung, R. Klett, A. Schmoldt, J. Cardoso, R. Montiel, M. H. Vazquez, L. Wang, F. Hosoi, H. Omichi, P. Goppelt-Langer, Carbonaceous clusters in irradiated polymers as revealed by UV-Vis spectrometry, Radiat. Eff. Defects Solids. 133 (1995) 193–208. https://doi.org/10.1080/10420159508223990.

[43] S. Ningaraju, H. B. Ravikumar, Ionic and electronic transport in PSF/NiO and PSF/TiO_2 polymer nanocomposites: A positron lifetime study, Solid State Ionics. 310 (2017) 81–94. https://doi.org/10.1016/j.ssi.2017.08.009.